SAND2012-0474C

Design and Direct Machining of Mesoscale Elastic Structures

ICOMM 2012 No.

Bradley H. Jared, Brad L. Boyce, Gerald A. Knorovsky, Lysle M. Serna
Materials Science and Engineering Center, Sandia National Laboratories, USA; e-mail: bhjared@sandia.gov•, blboyce@sandia.gov, gaknoro@sandia.gov, lmserna@sandia.gov

MOTIVATION

Traditional coil wound springs present a barrier to the miniaturization of mechanical mechanisms because uncertainties in forming processes introduce unacceptable performance margins for spring wire diameters smaller than 100µm. Dimensional errors, process tooling damage and material variances each contribute to excessive margins which drive subsequent design compromises. Such compromises are antithetical to the intentions of miniaturization as mechanism characteristics such as mass, volume, contact stress, actuation force and power consumption are commonly increased to accommodate manufacturing limits. An alternative approach under investigation involves the design of meso scale elastic structures that are fabricated, not by forming, but through direct machining methods. Inspired by medical stents [1], these miniature elastic elements introduce new design freedoms relative to materials, geometry, performance, functionality and manufacturing. The present work has examined the new design space introduced by direct machining and the trade-offs and optimizations necessary to satisfy performance requirements for a three-dimensional coil spring. Micro-wire EDM and pulsed laser machining have each been investigated as direct machining processes since their accuracy, resolution and minimal material impacts satisfy requirements for the generation of meso scale spring structures with improved repeatability, manufacturability and reliability over coil wound springs. While medical stents represent a baseline for springs operating at the meso scale, their primarily radial motion across a relatively small range of motion demands material, design and process requirements than are dramatically different from the current work.

SPRING DESIGN

The design of coil would springs is relatively restrictive as geometries must adhere to forms constrained by a constant wire cross-section that must be plastically deformed into a desired shape without exceeding material failure stresses. The utilization of a direct machining process significantly reduces geometry restrictions based on material strength, essentially enabling any geometry that can be realized based on an initial material form and machining capabilities (i.e. accuracy, material access, axes of motion, etc.). As a result, geometries leveraging features such as multi-start or variable cross-section elements can be generated to balance end moments, introduce structural redundancy, reduce stress concentrations (i.e. particularly for end tangs), or simultaneously tailor dynamic and static load responses. Direct machined springs already exist at the macro scale [2], and serve applications that require their increased functionality and/or accuracy.

Fig. 1: Prototype meso scale extension spring on a penny.

In order to understand the design space introduced by direct machining at the meso scale and to demonstrate its viability for small springs, a structure was designed based on the requirements for a coil wound extension spring utilizing 50 µm diameter wire. The initial design geometry in Fig. 1 relied on a single start, three-dimensional coil similar to a traditional coil wound spring. Design forms that were considered within the relaxed constraints of direct machining included a straight cantilever beam flexure, a planar spiral spring and a helical coil spring. While a cantilever provides the highest natural frequency for an equivalent stiffness, it requires a footprint and subsequent operating volume that are roughly an order of magnitude larger than the helical geometry. Similarly, the equivalent planar spiral spring requires a 5x larger footprint than the helical spring and produces a first mode resonance that is roughly one third lower. As expected from its ubiquitous and historical use across a wide range of engineering applications, the helical coil spring provides the most compact structure balancing design requirements for achieving a desired stiffness, for maintaining a uniformly distributed stress field below the material yield strength, and for maximizing the natural frequency. The rectangular cross-section of a machined coil spring also provides a form that minimizes spring volume for a desired stiffness, although the circular cross-section of a coil wound spring is the optimal shape to minimize loading stresses.

• corresponding author

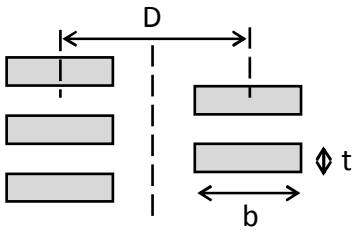

Fig. 2: Spring cross-section notation.

The design of a direct machined meso scale helical spring was performed based on operating requirements that specify the required spring forces, F_1 and F_2, at their respective operating deflections, δ_1 and δ_2. Working volume constraints define the maximum outside spring diameter, $D_{o,max}$, and/or the minimum inside spring diameter, $D_{o,min}$, Fig. 2. A general guideline for the maximum working stress in extension springs is that it should not exceed 45% of the ultimate material tensile strength [3]. While the material with the largest tensile strength is obviously desired for any application, additional requirements (ex. temperature, corrosion resistance, etc.) typically drive material selection and the subsequent maximum operation stresses.

The required spring stiffness, k, was found from the simple relationship

$$k = \frac{F_2 - F_1}{\delta_2 - \delta_1} \tag{1}$$

The stiffness of a helical spring design with a rectangular cross-section can then be predicted by the relationship

$$k = \frac{4G \cdot t^4}{3\pi \cdot D^3 \cdot N}\left(\frac{b}{t} - 0.627 \cdot \tanh\frac{\pi \cdot t}{2b} + 0.004\right) \tag{2}$$

which was developed [4] using closed form solutions and empirical data from Wahl [5] where the spring coil width, b, was assumed to be larger than its thickness, t. G represents the spring material shear modulus, while N is the number of spring coils and D is the mean coil diameter, Fig. 2. The working stress in the spring due to the operating load, P, was also developed by Wahl [5] and can be presented in the form

$$\tau = \frac{P \cdot D(3t + 1.8b)}{2t^2 \cdot b^2}\left(1 + \frac{1.2t}{D} + \frac{0.56t^2}{D^2} + \frac{0.5t^3}{D^3}\right) \tag{3}$$

A first mode natural frequency, ω_n, of the spring was also considered during the design process and can be approximated as

$$\omega_n = \frac{1}{2\pi}\sqrt{\frac{k}{\rho \cdot t \cdot b \cdot \pi D \cdot N}} \tag{4}$$

where ρ is the spring material density.

A closed form optimization using (1-4) was considered during the design process, but determined prohibitive due to the complexity of the nonlinear constraint equations. Therefore, design curves were instead generated in MATLAB. The

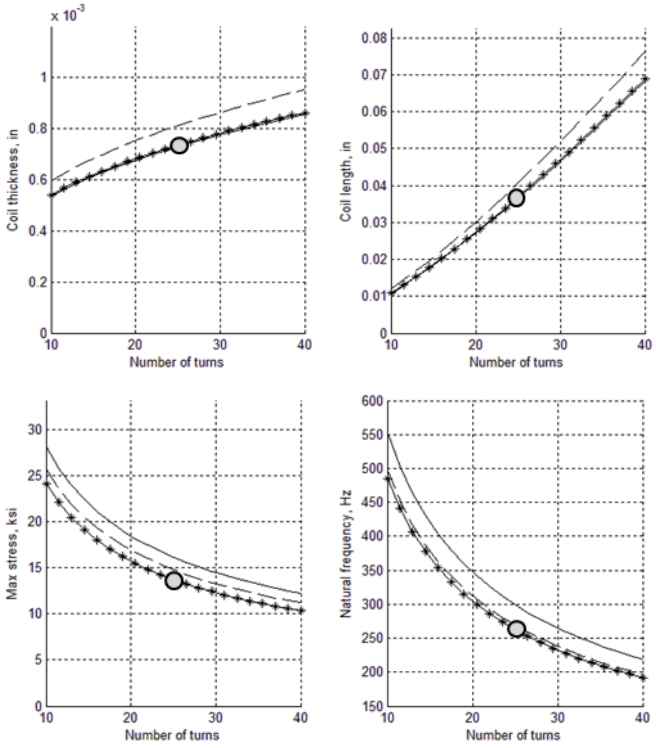

Fig. 3: Design charts for spring design showing a) coil thickness, b) coil length, c) working stress, and d) natural frequency.

coil thickness necessary to achieve the targeted spring stiffness was solved numerically from (2) using a simple bisection root solver. Subsequent design curves, Fig. 3, were generated based on a range of coil turns and tubing sizes that fit within the diameter constraints of the design. Fig. 3 shows curves for the tubes with the three largest outside diameters since they represent the designs with the lowest working stresses. Since hypodermic needle tubing was used as the base spring material, only readily available, stock vendor tube sizes were considered in the analysis. While this discretization of potential coil widths and diameters restricted the design process, most vendors can provide custom sizes upon request that would improve spring performance. The final design attempted to balance a coil thickness that could be achieved in fabrication, minimum active coil lengths and working stresses, and a maximum first mode resonance. The final design, represented by the circles in Fig. 3, uses 25 coils, an inside diameter of 0.58 mm, an outside diameter of 0.89 mm, a coil thickness of 40 μm and a coil spacing of 65 μm. Its resultant working stress is 94.5 MPa with a natural frequency of 262 Hz. The closed form design was then compared against a finite-element model and found to agree within 10% of one another in terms of predicting spring stiffness and natural frequency. While the closed form predictions were expected to primarily capture design trends for meso structures, experimental data from prototype springs has demonstrated agreement to within 5% of predictions, as will be discussed later. Fig. 4 compares the prototype meso spring design with its coil wound equivalent. While the coil wound spring has the higher natural frequency by approximately 25%, the directly machined spring provides the opportunity for a smaller

overall

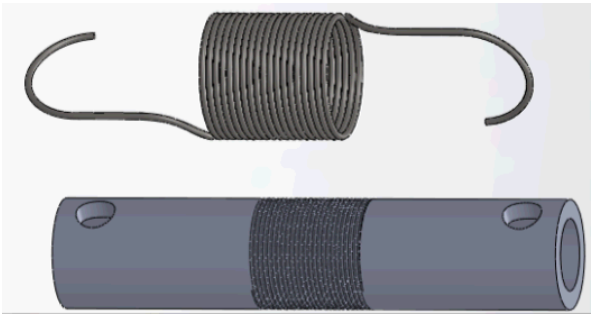

Fig. 4: A meso spring compared to its coil wound equivalent.

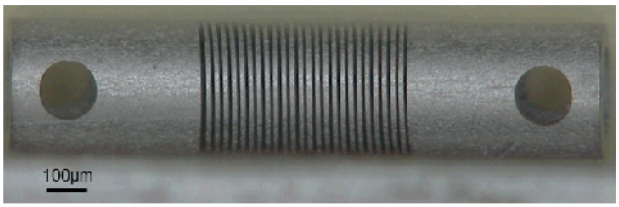

Fig. 5: Prototype meso spring.

spring volume. Moreover, its end geometry eliminates the end tangs which are a common failure point in wound springs and a restriction to assembly processes.

MATERIAL SELECTION

For any spring application, the general material requirements include a large elastic modulus, a high yield strength, isotropic mechanical properties, ductility and a linearly elastic response across the range of operating stresses (i.e. no microplasticity, ratcheting or low-cycle fatigue). Long term and high temperature stability are also required in some applications. For meso springs, an additional requirement is the presence of grain sizes small enough such that multiple grains span the load bearing features in the structure (typically < 5 µm). 304L grade stainless steel hypodermic needle tubing was utilized as the base material during the present design studies due to its commercial availability from the medical industry and its well characterized material properties. Although 304L is not considered a classical spring material due to its moderate yield strength (approximately 520 MPa), its microstructure can be controlled to achieve the grain structures necessary for meso springs, and its performance has proven better than anticipated, as described in the final section.

MESO SCALE FABRICATION

While macro scale machined springs may rely on traditional machining methods, the fabrication of meso scale springs with structural elements smaller than 50 µm requires greater accuracy, higher resolution and minimized material impacts from the machining process. Micro-wire EDM and pulsed laser machining have each been examined due to their ability to generate features at the 5-10 µm scale with process accuracies on the order of 1-5 µm. As an example, Fig. 5 shows a prototype meso spring based on the described design that was laser machined from stock 304L hypodermic needle tubing. Since the desired spring geometry can be described easily by a cylindrical coordinate form, springs are cut in a 3-axis configuration where the tube is spun in θ about its length axis by a

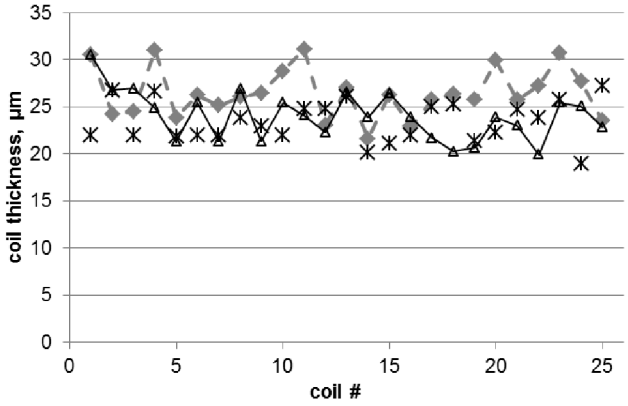

Fig. 6: Coil thickness data from prototype meso springs.

rotary stage. The rotary stage is mounted onto a stacked XY linear stage which then enables coordinated positioning of the tube to any position along its length or depth relative to a stationary laser focal point. Fig. 6 provides data from three different prototype springs from the same lot where the average coil thickness is 25 µm with a range of 12 µm and a standard deviation of 2.8 µm.

One unique challenge in the direct machining of meso springs is the energy input that occurs in any subtractive process whereby surface layers are generated due to heat affected zones (HAZ), recast, etc. Although recast and the white layer have been examined in conventional wire EDM [6], minimal research has been found regarding surface layers in micro-wire EDM [7]. Similarly, claims for ultra-fast, femtosecond pulsed lasers suggest negligible thermal effects during material removal near the ablation threshold [8], but not in higher fluence regimes where fabrication processes are typically performed to achieve adequate throughputs [9]. Therefore, work was performed to quantify and minimize the material damage layers generated during fabrication of a meso scale elastic structure.

Line cuts were performed in 250 µm thick, annealed 304L shim stock across a range of process parameters using a micro-wire EDM, a nanosecond pulsed laser and a femtosecond pulsed laser. The samples were then cross-sectioned for optical microscopy to evaluate the heat affected zones generated at the cut surfaces. Fig. 7 shows a representative cross-section from a nanosecond pulsed laser using a 6 ns pulse duration, a 14 kHz repetition rate, a 0.19 mJ energy per pulse, a 0.1 mm/sec scan velocity and 20 machining passes. The large 15-20 µm melt zone is clearly unacceptable for meso spring fabrication, and therefore precluded a ns laser from further fabrication considerations. Fig. 8 shows the cross-section from a femtosecond laser with a 100 fs pulse duration, a 1 kHz repetition rate, a 0.46 mJ pulse energy and the same scan velocity and number of passes as for the nanosecond laser. A superior cut is clearly achieved with a HAZ region on the order of only 1-2 µm. Given the converging nature of the focused laser beam, straight side walls

are only achieved at the exit of the cut with taper occurring at the top side of the cut. Fig. 9 shows the cut obtained from the micro-wire EDM using

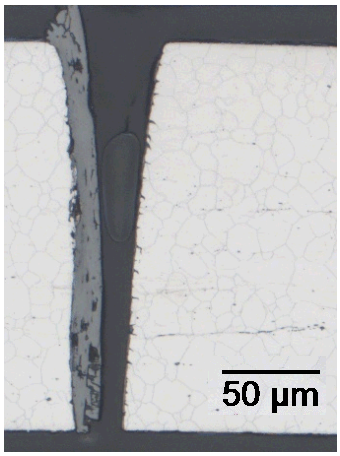

Fig. 7: Cross-section and heat affected zone in 304L from a nanosecond pulsed laser.

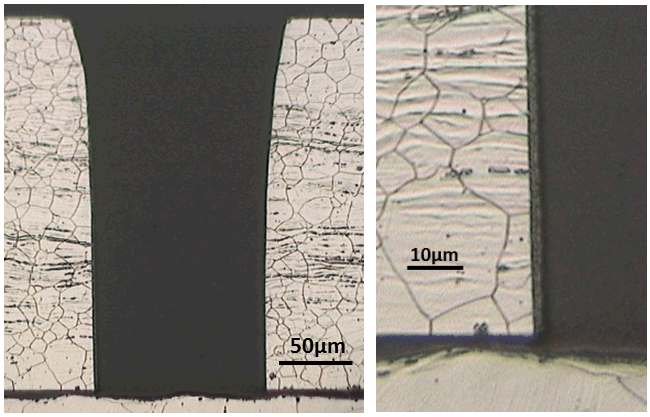

Fig. 8: Cross-section and heat affected zone in 304L from a femtosecond pulsed laser.

a 20 µm diameter tungsten wire. The left side of the cut represents the initial roughing pass, while the right surface was achieved using eight finishing passes. Similar to the femtosecond laser, a HAZ less than 1-2 µm is produced, although, unlike the laser, straight side walls are achieved through the entire depth of cut. While a 1-2 µm damage layer might not appreciably affect the elastic modulus and hence the static spring stiffness, its presence combined with the surface roughness generated by the fabrication processes will reduce the fatigue strength of structures at the meso scale. Therefore, a parallel effort has been performed to examine an electropolishing step applicable for meso scale springs with high aspect ratio features [10].

PROTOTYPE SPRING PERFORMANCE

Over 50 meso springs have now been fabricated using pulsed laser machining per the initial design described in the first section. Fig. 10 shows measured stiffness values from 20 springs compared to calculated spring rates using the closed form relationship (2) and measured spring geometries from the respective springs. Measured stiffness variations of only 10% have been observed with agreement against the closed form predictions to within 5%. The accurate measurement of coil thickness has proven critical in predicting spring behavior, as thickness variations have been observed to be

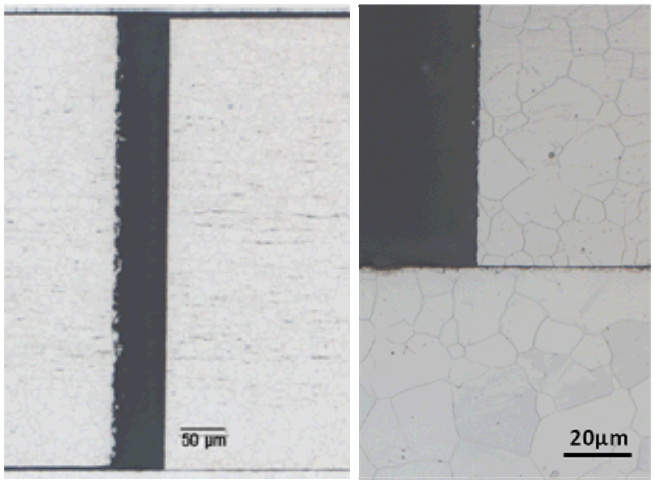

Fig. 9: Cross-section and heat affected zone in 304L from a micro-wire EDM.

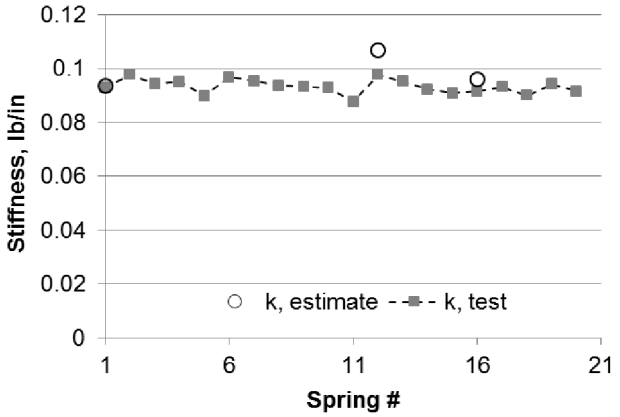

Fig. 10: Prototype meso spring experimental stiffness data and closed form model predictions.

approximately 10% and to correlate directly with measured stiffness values. Preliminary fatigue tests have also proven successful with as-machined structures demonstrating fatigue life up to 1 million cycles under loading conditions. An order of magnitude improvement in fatigue life has also been observed with the introduction of electropolishing.

CONCLUSIONS

The design, fabrication and performance of a directly machined meso scale extension spring has been demonstrated as an alternative to traditionally wound coil springs. A three-dimensional helical spring geometry was determined to meet spring requirements within a minimum working volume and footprint. Closed form relationships were used to generate design curves in MATLAB from which the prototype design was determined based on a balance of coil thickness, active coil length, working stress and natural frequency. Good correlation was observed between the closed form solutions and a finite element analysis. 304L was selected for the spring material as investigations of cut quality and heat

affected zones were performed using a nanosecond laser, a femtosecond laser and micro-wire EDM. Prototype springs were then fabricated based on the baseline design using pulsed laser machining. Evaluation of the prototype springs has shown stiffness variations of only 10% with agreement against closed form predictions to within 5%.

ACKNOWLEDGMENTS

Sandia National Laboratories is a multi-program laboratory managed and operated by Sandia Corporation, a wholly owned subsidiary of Lockheed Martin Corporation, for the U.S. Department of Energy's National Nuclear Security Ad-ministration under contract DE-AC04-94AL85000. This document has been reviewed and approved for unclassified, unlimited release under SAND2012-xxxxA.

REFERENCES

[1] D. Stoeckel, C. Bonsignore, S. Duda, "A Survey of Stent Designs," *Min. Invas. Ther. & Allied Tech.*, 2002; v11 n4: 137-147.

[2] G.L. Boehm, "Which Spring to Choose: Coiled Wire vs. Machined, a Comparison," *Mech. Eng.*, August 2010; web exclusive.

[3] Design Handbook: Engineering Guide to Spring Design, Associated Spring: 1987, 52.

[4] W.C. Young, Roark's Formulas for Stress & Strain, McGraw-Hill: 1989, 386-387.

[5] A.M. Wahl, Mechanical Springs, McGraw-Hill: 1963, 124-130.

[6] A.B. Puri, B. Bhattacharyya, "Modeling and Analysis of White Layer Depth in a Wire-Cut EDM Process Through Response Surface Methodology", *Int. J. Adv. Mfg. Tech.*, 2005; 25: 301–307.

[7] G.L. Benavides, L.F. Bieg, M.P. Saavedra, E.A. Bryce , "High Aspect Ratio Meso-Scale Parts Enabled by Wire Micro-EDM", *Microsystem Tech.*, 2002; 8: 395–401.

[8] B.N. Chichkov, C. Momma, S. Nolte, F. von Alvensleben, A. Tunnermann, "Femtosecond, Picosecond and Nanosecond Laser Ablation of Solids", *Appl. Phys. A,* 1996; 63: 109-115.

[9] G. Kamlage, T. Bauer, A. Ostendorf, B.N. Chichkov, "Deep Drilling of Metals by Femtosecond Laser Pulses"", *Appl. Phys. A*, 2003; 77: 307-310.

[10] L.M. Serna, B.L. Boyce, B.H. Jared, "Electropolishing Effects on Surface Roughness of Direct Machined Simulated Coil Gaps", *ICOMM*, 2012.